Available online at www.sciencedirect.com
SCIENCE DIRECT®
Journal of Sound and Vibration 286 (2005) 897–920
JOURNAL OF SOUND AND VIBRATION
www.elsevier.com/locate/jsvi

Compensation for encoder geometry and shaft speed variation in time interval torsional vibration measurement

Brian R. Resor[a], Martin W. Trethewey[a,*], Kenneth P. Maynard[b]

[a]*Department of Mechanical and Nuclear Engineering, Penn State University, 336 Leonhard Building, University Park, PA 16802, USA*
[b]*Applied Research Laboratory, Penn State University, University Park, PA 16802, USA*

Received 17 November 2003; received in revised form 4 October 2004; accepted 24 October 2004
Available online 18 January 2005

Abstract

Digital time interval techniques for the measurement of torsional vibrations in rotating shafts have been used in a variety of applications. The techniques use high-speed timers to detect the passage times (often referred to as "zero crossings") in a carrier signal from a multiple pulse per revolution encoder on the shaft. Next, a reference array is created by computing the passage times for an encoder with geometrically uniform segments rotating at a constant speed. The measured times are compared against the reference array and the time difference processed to yield the shaft torsional vibration. If the reference array differs from the encoder passage times, the calculated torsional vibration will be subject to bias errors manifested as high-level order content. There are two potential causes for inconsistency in the reference signal: (1) geometric variation in angular encoding device and (2) a non-constant shaft speed. Procedures to handle these situations are addressed. An in situ encoder calibration method is presented that creates a reference array representative of the actual encoder angular intervals. The method uses time synchronous averaging of the encoder zero crossing over many shaft revolutions. The process causes the time passage variations induced by the torsional vibration to average to zero, ultimately yielding the time stamps caused by the passage of each respective encoder segment. The synchronous averaged encoder passage times are then used to correct the reference array to calculate the torsional vibration. Variation of the encoder geometry and changes in shaft running speed cause the torsional vibration be sampled on a non-uniform time interval basis. The non-uniform time sampling would cause errors if used with fixed sampling interval algorithms such as the DFT. A resampling algorithm is applied to create an array sampled with a constant time interval basis to minimize the error. The background and implementation details of time interval torsional

*Corresponding author. Fax: +1 814 865 9693.
E-mail address: mwtrethewey@psu.edu (M.W. Trethewey).

0022-460X/$ - see front matter © 2004 Elsevier Ltd. All rights reserved.
doi:10.1016/j.jsv.2004.10.044

Nomenclature

f_{clock}	zero crossing detection clock speed (Hz)
$f_{shaft}(j)$	shaft running speed for jth revolution (Hz)
$f_{shaft,avg}$	average shaft running speed over multiple revolutions (Hz)
j	revolution index
m	constant time sample index
n	encoder segment index
N	number of encoder segment
o	order
$r_j(n)$	time passage ratio for nth encoder segment during jth revolution
$r(n)$	averaged time passage ratio for nth encoder
$t(n)$	reference time for passage of nth identical geometry encoder segment at constant speed without any torsional vibration (s)
$t_{ref}(n)$	zero crossing reference time for nth encoder segment (s)
$t_{encoder}(n)$	zero crossing time for nth encoder segment (s)
$\Delta t(n)$	time difference between reference and nth encoder segment passage (s)
$\Delta t_{sample}(n)$	constant time sampling interval (s)
$\Delta t_{clock}(n)$	zero crossing detection time interval (s)
$\Delta t_{corrected}(n)$	corrected zero crossing detection time interval (s)
$T(j)$	period for the jth revolution (s)
α_n	angular sampling increment (deg)
θ	torsional vibration (deg)
Θ	order domain discrete Fourier transform of torsional vibration

vibration measurement enhancements are first presented. The capabilities are then demonstrated with experimental results from several pieces of rotating equipment. The tests show the successive improvement in the torsional vibration data as the proposed compensation methods are sequentially applied.
© 2004 Elsevier Ltd. All rights reserved.

1. Introduction

The measurement of torsional vibration is important in analysis and diagnostics of rotating equipment. Applications are plentiful, including the automotive [1–3] and the electrical power industries [4–6]. The measurement of torsional oscillations on a rotating shaft is inherently more difficult than translational vibration. As such, a significant amount of work has been devoted to developing effective torsional measurement techniques and has produced a variety of schemes. The reported methods include the use of lasers [7,8], in line torque sensors [9], angular accelerometers [10] and time passage encoder-based systems [11–13].

Recently, many applications have utilized encoder-based systems. The methods use a fixed angular encoding device that rotates with the shaft such as a gear or optical rotary encoder. A transducer is then used to sense the passage of each encoder segment with respect to a reference point as the shaft rotates. Optical encoders use a light-based system to sense the passage of a rotating grating. Previous applications of gear-type shaft encoder systems have used a number of transducers including Hall effect, fiber-optic reflective light intensity, inductive and capacitive sensors. Regardless of the sensing system used, the output is a pulse train type signal in which the

passage times vary as a function of the shaft rotation and the torsional oscillation. The processing of the passage times to obtain the torsional vibration can be separated into two general categories: (1) an analog approach [14] and (2) a digital time interval measurement (TIM) approach [15]. Both methods rely on the accurate sensing of the encoder segments' passage to determine the torsional vibration. The analog method uses a frequency to voltage converter to change the pulse train into an analog signal proportional to the vibration. The digital method uses a high-speed timer to record the passage of each encoder segment. The encoder passage times are then compared to a reference for the shaft at a constant speed without any torsional oscillation. The time difference between the encoder and the reference signal is used to compute the torsional vibration.

A typical time interval measurement system used for torsional vibration is seen in Fig. 1. The encoding device can be a toothed gear, a striped disk, or an optical encoder. The transducer output is a high or low voltage depending on whether it detects "white" or "black" regions of the transducer segments. If the shaft rotates at a constant rate in the absence of any elastic torsional vibration a periodic carrier wave is produced. When torsional vibration occurs in the shaft, it causes a fluctuation in the rotating shaft speed. Therefore, the transducer output signal is a carrier wave with a fundamental frequency related to the passage rate of encoder pulses modulated by the torsional vibration angular motion. A time interval measurement approach can be used to demodulate the torsional vibration from the carrier wave [15]. The technique is based on the encoder segments' passage times with respect to a stationary transducer. Fig. 2(a) depicts a nominal reference signal with the assumptions of (1) a uniform interval encoder with N equal segments, (2) a constant rotational speed, f_{shaft} (Hz), and (3) no elastic torsional oscillation. A hypothetical triggering sensor is used to record the times when the reference signal has a zero value with a negative slope. Note, the term "zero crossing" is used for descriptive purposes since it is feasible to set other timer trip voltage levels (i.e., 2.5 V for a TTL signal). An array containing the negative slope zero crossing times (t_{ref}) may be computed by

$$t_{\text{ref}}(n) = \frac{n}{N f_{\text{shaft}}}(s), \quad 1 \leqslant n \leqslant N. \tag{1}$$

Fig. 2(b) shows the encoder output when the shaft is rotating at a constant speed while experiencing elastic torsional oscillations. When the negative slope zero crossing detection is applied to the encoder signal, an array (t_{encoder}) indicative of respective passage times is created.

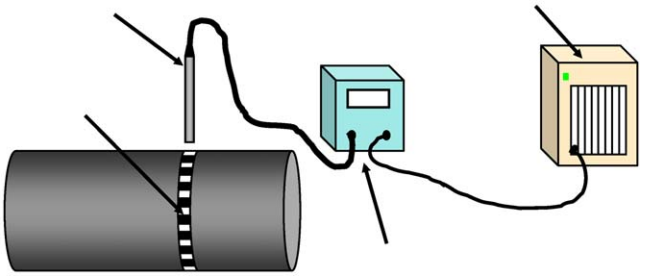

Fig. 1. A digital time interval torsional vibration measurement system.

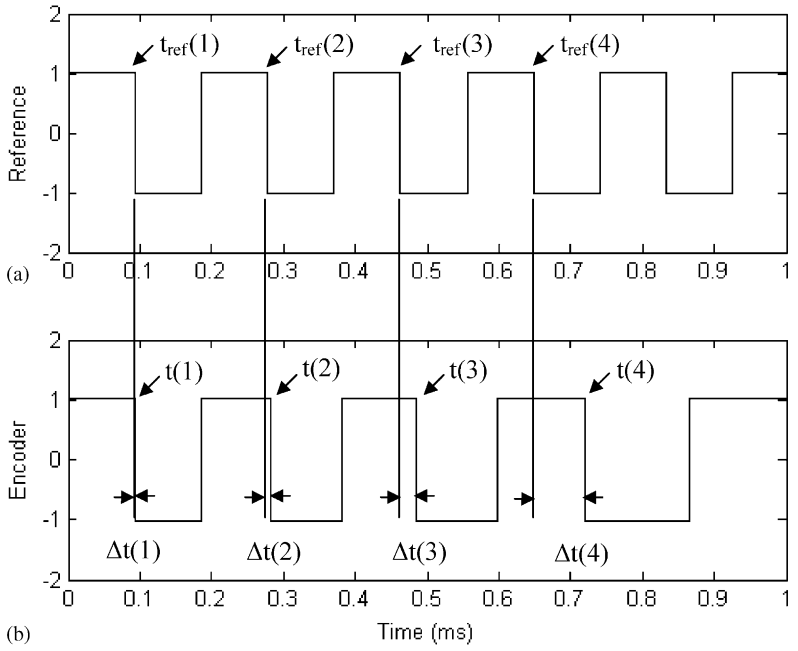

Fig. 2. (a) Reference and (b) encoder signals from a rotating shaft experiencing elastic torsional oscillations.

The difference between the encoder and reference zero crossing times are computed by Eq. (2):

$$\Delta t(n) = t_{\text{encoder}}(n) - t_{\text{ref}}(n) \quad \text{(s)}. \tag{2}$$

The angular variation due to the vibration, in degrees, can then be calculated from the time difference array:

$$\theta(n) = \Delta t(n) f_{\text{shaft}} 360 \quad \text{(deg)}. \tag{3}$$

Eq. (3) can be used to create a discrete array containing the torsional vibration amplitude at the respective time corresponding to passage of each encoder segment. Since the shaft is assumed to rotate at a constant speed and an equal segment encoder is employed, the array is sampled on a uniform angular increment basis. With the assumption that the time interval associated with the torsional vibration is much smaller than that due to the shaft rotation, a constant time sampling interval corresponding to the angular increments is

$$\Delta t_{\text{sample}} = f_{\text{shaft}} N. \tag{4}$$

By combining Eqs. (3) and (4) the shaft torsional vibration sampled with a constant interval time basis over one revolution becomes

$$\theta(t(n)) = \theta(n), \tag{5}$$

where

$$t(n) = \Delta t_{\text{sample}} n. \tag{6}$$

Although theoretically feasible, this measurement procedure has several potential problems [11,12,16].

1. *Reference signal corruption*: the ideal encoder reference expressed in Eq. (1) assumes (1) an encoder with exactly equal geometric segments, and (2) a constant rotational speed. In practice, both these assumptions are usually violated causing errors in reference signal used to compute the torsional vibration.
2. *Non-uniform sampling intervals*: any variations in encoder segment geometry cause the torsional vibration signal to be sampled on a non-uniform angular increment basis. Furthermore, Eq. (4) assumes the shaft speed is constant. During normal operation the shaft speed can change for two reasons: (1) inherent operation of the drive motor, and (2) torsional oscillations in the shaft. These conditions can combine to cause the torsional vibration to be sampled on a non-uniform interval basis (both angular and time). Therefore, spectral analysis using constant interval algorithms such as the discrete Fourier transform is problematic if not precluded depending on the severity.
3. *Timer resolution*: the derivation of Eq. (2) is based on the assumption that is possible to resolve infinitesimally small time differences between the reference and encoder signals. However, the achievable time resolution is governed by the clock rate used in the zero crossing detection circuit. The clock rate affects the angular resolution of the measurement system.
4. *Transverse shaft movement*: if the transducer experiences any lateral movement with respect to rotating shaft the zero crossing times will be corrupted inducing errors in the torsional vibration.

Previous work has addressed many of these identified errors, including lateral vibration [12] and processing issues [16]. The work presented herein will focus on errors induced by non-uniform shaft encoders (Item 1) and variation in shaft running speed (Item 2). An investigation into the character of each respective item will be discussed first. Methods to compensate each item are then presented and evaluated. Experiments are performed on both a laboratory test bed and industrial rotating equipment to illustrate the proposed methods' capabilities to improve the torsional vibration measurement quality.

2. Shaft encoding

The reference signal expressed in Eq. (1) assumes a transducer with an integer number of equal dimension encoder segments around the shaft. In practice, this is difficult to achieve. A number of different types of encoding device have been used previously. The most desirable is a precision optical encoder since the high accuracy manufacturing provides incremental segments that are virtually identical, differing by only a very small tolerance. Unfortunately, it is not always possible to use high-quality optical devices. This is particularly true when retrofitting existing equipment to measure torsional vibration. Alternative encoder systems suitable for retrofitting are gears, split ring collars with machined teeth or zebra tape. Gears have been used in a number of applications [13], including a jet engine test cell [17]. A striped "zebra tape" printed on adhesive paper and applied to the shaft is an attractive alternative due to its simplicity. Zebra tape applications

include hydro-power plants [6], NASA-Ames Full-Scale Aerodynamic Complex wind tunnel fan drive shafts [17] and laboratory test beds [12,17]. The geometric variation between encoder segments of these shaft encoding devices is much greater than high precision optical devices and has the potential to induce significant errors in the computed torsional vibration signal.

In Ref. [16], the error in the torsional vibration caused by tooth spacing variation was simulated. In the simulation, it was assumed that the tooth spacing could be represented by a Gaussian distribution with three standard deviations equal to the American Gear Manufacturers Association (AGMA) maximum geometric tolerance for a specific gear rating class. The spacing tolerance was shown to induce a broadband error that affects the angular measurement noise floor. As the AGMA gear rating increased (smaller geometric error tolerances) the torsional vibration noise floor decreased. Furthermore, since the spacing pattern in the gear repeats each revolution, the error manifests itself as high-level content at integer multiples of the shaft running speed or in other words, integer orders.

The use of zebra tape around a shaft induces problems associated with printing unevenness, installation misorientation and operational changes. Ideally, there are exactly an integer number of equidistant alternating black and white sections around the tape on the shaft circumference as depicted in Fig. 3(a). Most printers work by laying down lines of ink or toner as the sheet feeds past the print head. The line width is fixed depending on the printer resolution. If the desired printed stripe width is not an integer multiple of the print resolution, then some stripes will have more toner lines than others due to printer round-off. The unevenness of the printer segments can be further affected by the installation of the tape around shafts. Often when the zebra tape is wrapped around a shaft the ends do not exactly match, creating either a slight larger or shorter segment at the joint. Fig. 3(b) is an exaggerated depiction of a tape with printing and end effects errors. The tape also needs to be installed with the printed lines parallel to the shaft's rotational axis. Such a precise tape installation can be problematic, particularly on large diameter shafts. An imprecise installation induces slight positional orientation errors that affect the uniformity of the

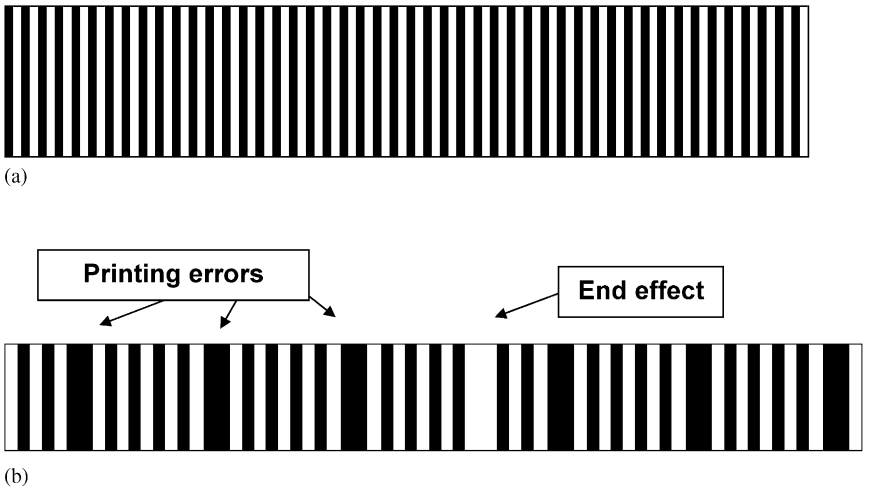

Fig. 3. Examples of printed zebra tapes for torsional vibration measurement: (a) equally spaced white and black segments; (b) exaggerated effects from printer resolution and installation end effects.

tape segments as measured by the transducer. Furthermore, thermal expansion from normal equipment operation can affect the tape dimensions. Thermal growth can change the tape width and end overlap dimensions.

These issues highlight the difficulty in using zebra tape as an encoding device. However, the ease at which zebra tape can be used has motivated investigations to try and correct for these identified difficulties. Vance suggests fixing the problem by recording "noise" at a constant speed (no torsional excitation) and subtracting it later in the signal processing routine [15]. Williams proposes that the stationary nature of the errors can be used to identify the random pattern caused by tooth spacing error [16]. However, no procedure is provided to perform the identification and correction. Wang et al. [12] describes a technique very similar to that proposed by Vance [15]. Striped tapes were produced by a laser printer and variations in the stripe widths were suspected to cause a problem. To correct the problem, the ratio of each stripe width to the shaft circumference was measured with the motor running at a constant speed without torsional vibrations. The ratio measurements form a calibration file that is used for the torsional vibration computations. The approach functioned well, but the authors noted "for experimental situations where the shaft cannot be rotated at or near a constant speed, a special calibration procedure needs to be developed" [18]. The method's feasibility is further limited since it requires the equipment to operate without any torsional vibration to create the calibration file. This is particularly difficult to achieve in industrial applications, and hence application of the approach is precluded. Fu and Yan [11] describe a digital torsional vibration measurement technique that requires the use of a multiple pulse encoder. The technique claims to break through the requirement that the encoding devices be perfect. However, the development is cursory and no quantification of the method's capabilities is presented.

The errors induced by encoder geometry variation can be several orders of magnitude greater than the torsional vibration. Hence, any errors in the shaft encoding device can have a significant adverse effect on the measurement. Furthermore, most cited correction methods require the machine to run at a constant speed without torsional vibration. Therefore, a robust technique to characterize and correct for encoder non-uniformity and running speed variation in the digital torsional vibration measurement system is needed.

3. Geometric encoder characterization and correction

The reference signal expressed in Eq. (1) and shown in Fig. 2(a) assumes: (1) equal encoder segments; (2) constant shaft rotational speed, sans any torsional vibration, and (3) infinitesimal time resolution. Variations in encoder geometry and shaft speed cause these assumptions 1 and 2 to be violated. The reference should be formed from the zero crossing times from the actual encoder segments. To create a suitable reference, an in situ calibration method capable of correcting for the inherent geometric irregularities is proposed. The method is based upon synchronously averaging the zero crossing times for each respective encoder segment over many revolutions.

The calculation of the torsional vibration in Eqs. (2) and (3) assumed an infinitesimally small zero crossing detection capability. However, in practice the detection is usually performed with a high-speed timer/counter with clock rates, f_{clock}, between 20 and 100 MHz [11,17]. Therefore, the

discrete zero crossing time interval is the reciprocal of the clock speed.

$$\Delta t_{\text{clock}} = \frac{1}{f_{\text{clock}}}. \tag{7}$$

The timer/counter detects the zero crossings as the number of integer, n, time sample intervals (Δt_{clock}) observed from some starting reference. Therefore, the time corresponding to the nth zero crossing from the shaft encoder is

$$t(n) = n\Delta t_{\text{clock}} = \frac{n}{f_{\text{clock}}}, \tag{8}$$

where n represents the number of timer counts.

The time required for one revolution is determined by taking the difference between the times recorded for the successive passage of an encoder segment:

$$T_j = t((j+1)N) - t(jN), \tag{9}$$

where the array subscript, j, is the revolution index and begins with 1.

The time percentage of each encoder segment is first determined by assuming that the shaft speed remains constant throughout a single revolution. The normalized time passage ratio of encoder segment (n) for one shaft revolution is

$$r_j(n) = \frac{t((j-1)N + n + 1) - t((j-1)N + n)}{T_j}, \quad 1 \leqslant n \leqslant N. \tag{10}$$

Note, that the normalization period, T_j, is calculated for each respective revolution and is equal to the time it takes for one specific revolution. Values of $r_j(n)$ are then calculated for each encoder segment and averaged over M revolutions:

$$r(n) = \frac{1}{M}\sum_{j=1}^{M} r_j(n), \quad 1 \leqslant n \leqslant N. \tag{11}$$

Since the torsional vibration is not synchronized with the shaft rotation it can be viewed as an independent process with respect to encoder passage times. Therefore, averaging across many shaft revolutions forces the torsional vibration induced time increments to become zero, leaving only the systematic character of the passage times caused by the inherent encoder geometry and rotational speed. The averaged systematic character can then be used to correct for variations in the encoder geometry. The application can be seen by first combining Eqs. (1) and (2).

$$\Delta t(n) = t_{\text{encoder}}(n) - \frac{n}{Nf_{\text{shaft}}}, \quad 1 \leqslant n \leqslant NB, \tag{12}$$

where B is the total number of shaft revolutions. The shaft speed is assumed constant over each revolution index (j) and is computed from the passage time for the identical encoder segment (i.e., $n = 1$) during one revolution:

$$f_{\text{shaft}}(j) = \frac{1}{t(Nj+1) - t(Nj)}. \tag{13}$$

The average shaft rotation rate over B shaft rotations is thus

$$f_{\text{shaft,avg}} = \frac{1}{j}\sum_{j=1}^{B} f_{\text{shaft}}(j). \tag{14}$$

Combining Eqs. (12)–(14) yields the delta time passages

$$\Delta t(n) = t_{\text{encoder}}(n) - \frac{n}{N f_{\text{shaft,avg}}}, \quad 1 \leqslant n \leqslant NB. \tag{15}$$

Eq. (15) is computed with equal encoder segments. Therefore, the respective circumference ratio is the reciprocal of the number of encoder segments (N). The averaged encoder ratio can now be applied to Eq. (15) by multiplying the ratio of equal encoder segment ratio, $1/N$, to the measured encoder ratio, $r(n)$ in Eq. (11) over one revolution:

$$\Delta t_{\text{corrected}}(n) = \Delta t(n)\frac{1/N}{r(n)}. \tag{16}$$

The entire time difference array is corrected by sequentially applying Eq. (16) to the data from each respective revolution. As a result, these time intervals have been computed with respect to a reference that includes geometric variations in the encoder. By combining Eqs. (3) and (16) the torsional vibration can be calculated while compensating for encoder geometric variability between segments, i.e.,

$$\theta(n) = \Delta t_{\text{corrected}}(n) f_{\text{shaft}} 360 \quad (\text{deg}). \tag{17}$$

4. Torsional vibration sampling

The computed vibration amplitude occurs when the respective encoder segment passage is sensed. If the measurement process uses an ideal encoder with equal intervals, the torsional array is sampled on a constant angular basis $\theta(\alpha_n)$, where α_n is the angular sampling increment, or 360° divided by the number of encoder intervals (N). A discrete Fourier transform can be applied to constant angular sampled torsional vibration array $\theta(\alpha_n)$:

$$\Theta(o_r) = \sum_{r=0}^{N-1} \theta(\alpha_n) \mathrm{e}^{-\mathrm{i}(2\pi nr/N)} \tag{18}$$

to produce the order spectrum, which shows the signal content as multiples of shaft rotational speed. For a constant shaft running speed, there is a direct linear relationship between the angular and time-based sampling. Hence, the analogous frequency domain spectrum can be directly determined from the order spectrum.

Variations in encoder geometry cause the angular increments to be unequal. Furthermore, if the shaft speed is not constant there is not a direct relationship between the angular and time-based sampling. Hence, the times at which the torsional vibration is computed occur at non-constant time intervals as depicted in Fig. 4. The variation in sampling time increments is apparent. Therefore, the computed torsional vibration signal can be viewed as a signal that has been sampled on a non-uniform time basis or, in other words, a non-constant sampling frequency.

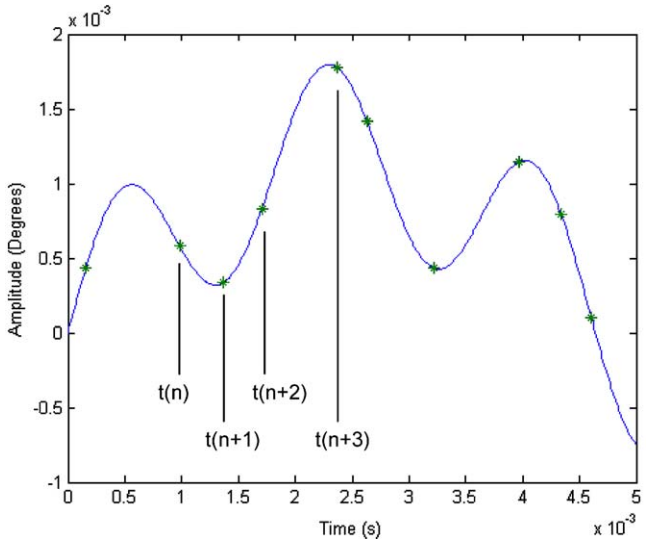

Fig. 4. Time basis torsional vibration discretization with non-uniform encoder and-or non-constant shaft running speed.

Since the discrete Fourier transform is based on a constant interval sampling, direct application to the irregularly time sampled torsional data yields results that are difficult to interpret.

A resampling of the torsional vibration signal is used to convert the array to a constant time interval basis, making it suitable for spectral analysis with the discrete Fourier transform. The resampling method is based upon the algorithm developed in Ref. [19]. Conceptually, the result of the process is depicted in Fig. 5, whereby the non-constant interval sampled array is interpolated to values that occur at constant intervals. The resampling method may be outlined as follows:

1. Using mean shaft speed from Eq. (14) and the number of encoder segments the average sampling frequency is computed as

$$f_{\text{s·avg}} = f_{\text{shaft}} N. \tag{19}$$

   The resampling frequency (f_{resample}) should be selected slightly greater than this value to avoid aliasing in the processed array. Otherwise, a low pass digital filter would have to be applied first.
2. A time array is created with a constant interval equal to the reciprocal of Eq. (20):

$$t_{\text{resample}}(m) = \frac{m}{f_{\text{resample}}}. \tag{20}$$

3. Recall that the computed torsional vibration measurements occur at the zero crossing times, t_{encoder} and correspond to the respective angular sampling intervals, $\theta(\alpha_n)$. This non-constant time interval sampled torsional vibration array is interpolated to obtain signal values at constant time intervals from Eq. (20). A cubic spline method is used to perform the interpolation [19].

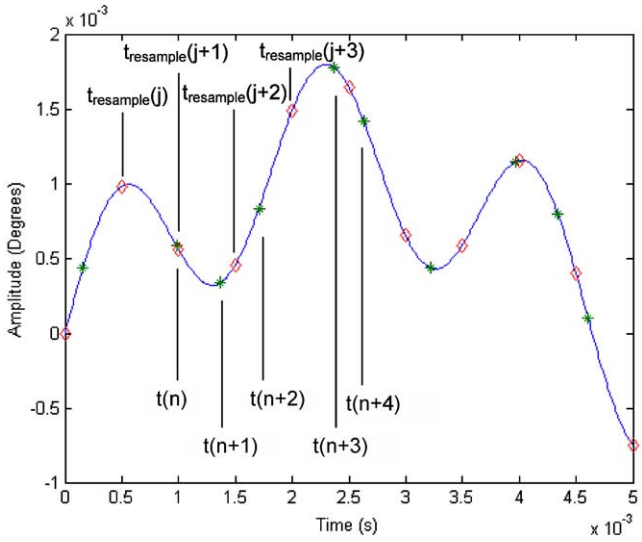

Fig. 5. Resampling of non-uniformly encoder sampled torsional vibration signal to a constant time interval basis.

The resampling process produces a torsional vibration array with a constant sampling interval, regardless of shaft speed and encoder geometry variation that occurred when the original time interval data was acquired.

5. Encoder compensation evaluation

To calculate the circumference ratio in Eq. (11), (1) the finite time resolution from the timer/counter clock rate; (2) the number of revolutions averaged, M; and (3) changes in shaft running speed during a single revolution are needed. To examine the sensitivity to these parameters, the data acquisition process was simulated and the compensation algorithm (Eqs. (11)) applied to the data. The output from an encoder with N equal circumferential segments for a rotational speed, f_{shaft}, is simulated by a square wave of fundamental frequency equal to Nf_{shaft} (Hz). Here N was chosen to be 180. The discrete time increment is the reciprocal of timer clock rate, f_{clock}. The passage times of the encoder segments are then computed by selecting the timer count that directly precedes the transition of the square wave from a positive to negative value. A sample of the encoder circumference ratio for one revolution is shown in Fig. 6(a). Although the segments are theoretically identical, the clock's finite resolution causes a one count variation in the zero crossing detection that then manifests itself as a difference in the computed circumference ratio. The mean and standard deviation of the N circumference ratios are then computed.

Next, Eq. (11) is implemented to examine the effects of averaging. A parametric evaluation was performed where the mean and standard deviation of the circumference ratio were computed for various increment encoders (N), shaft running speeds (f_{shaft}) and timer clock speeds, (f_{clock}). The range of the three variables was selected to represent nominal values used in applications. An

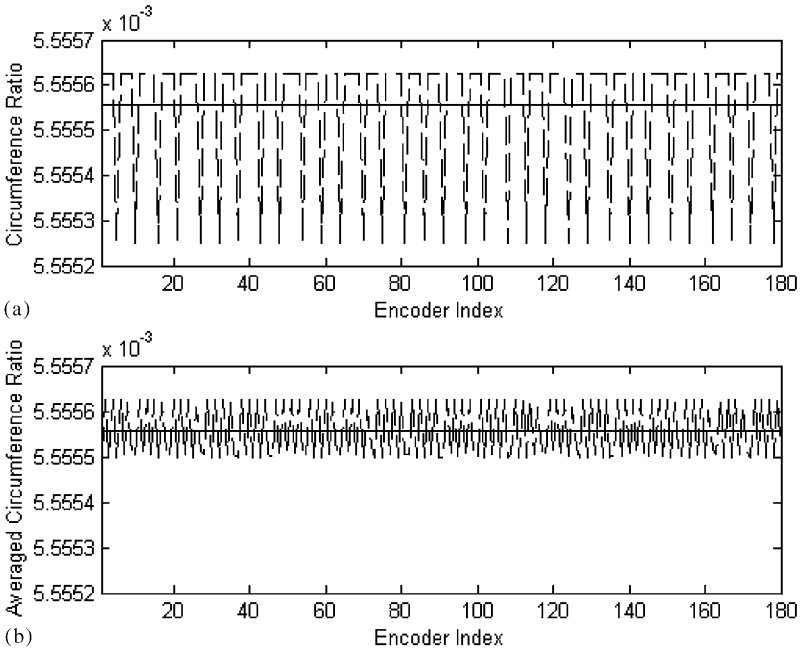

Fig. 6. Encoder circumference ratio computed from Eq. (11) with constant shaft speed with the operational specifications: encoder segments, $N = 180$; running speed, $f_{\text{shaft}} = 30\,\text{Hz}$; zero crossing clock, $f_{\text{clock}} = 80\,\text{MHz}$: (a) one revolution; (b) 50 revolutions; ——, actual value; - - - - - - -, computed from zero crossings.

Table 1
Standard deviation, normalized by theoretical segment, of the encoder circumference ratio computed from Eq. (8) with different averages with the operational specifications: encoder segments, $N = 180$; running speed, $f_{\text{shaft}} = 30\,\text{Hz}$; zero crossing clock, $f_{\text{clock}} = 80\,\text{MHz}$

Averages, M	Normalized standard deviation
1	2.63×10^{-5}
5	1.21×10^{-5}
10	1.13×10^{-5}
50	1.09×10^{-5}
100	1.09×10^{-5}

averaged circumference ratio using 50 revolutions is depicted in Fig. 6(b). The circumference ratio shows much smaller variations around the theoretical mean when compared to Fig. 6(a). It was found, see Table 1, that averaging more than 50 revolutions produced no increased benefit, with a standard deviation, normalized by the theoretical segment circumference, remained at 1.09×10^{-5}. These observations held true for all other operating conditions simulated. Therefore, it is recommended that 50 revolutions be used in the averaging process.

Eq. (11) was developed with the assumption that the shaft running speed remained constant throughout each revolution. The sensitivity to this assumption can be evaluated by allowing the

shaft speed to be a function of time in the simulation. The shaft speed was assumed to vary sinusoidally around a nominal value, with the amplitude and revolutions/min change rate as variables. Since the acquisition of the data for 50 revolutions is nominally less than several seconds, it is expected that the actual change in running speed will be small during this time frame in actual applications. Fig. 7 shows a typical shaft speed variation over the time required to capture the 50 revolutions. The standard deviation of the circumference ratio, normalized by the theoretical value, was computed for a number of revolutions/min amplitude variations and rotational rates of change. A compilation of sample results for several speed variation conditions is shown in Table 2. The normalized standard deviation of the circumferential ratio is nominally less than one half that computed for constant speed operation (Table 1). The changing shaft speed can be beneficial in the averaging process under some conditions. The changing shaft speed tends to more randomly distribute the actual zero crossing within the available timer resolution increment and decreases the standard deviation. Somewhat different results were observed in simulations of the high-speed turbo-machinery conditions in Ref. [17] where the shaft speed changed as much as 200 revolutions/min in 120 shaft revolutions. In this case the standard deviation when compensation is based on averaging fifty revolutions with the speed change was approximately double that obtained for a single revolution at a constant speed.

For all the operating conditions simulated the results were similar. The standard deviation of the circumference ratio for simulated operating conditions was similar (i.e., 50 averages with

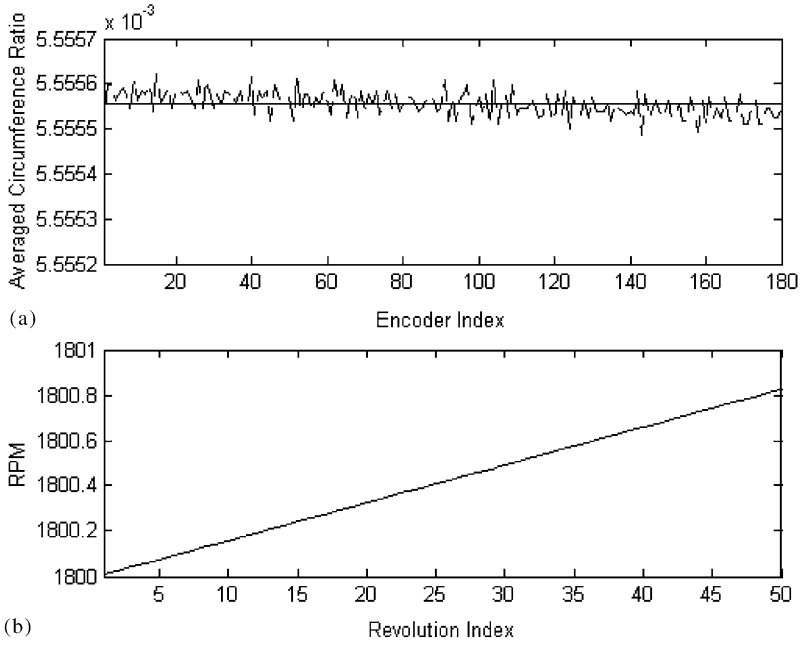

Fig. 7. (a) Encoder circumference ratio computed from Eq. (11) with changing shaft speed for 50 revolutions with the operational specifications: encoder segments, $N = 180$; running speed, $f_{\text{shaft}} = 30$ Hz: Zero crossing clock, $f_{\text{clock}} = 80$ MHz. ——, actual value; - - -, - - - - computed from zero crossings. (b) Shaft revolutions/min with respect to the revolution average index. Shaft running speed specifications: nominal = 1800 revolutions/min, variation amplitude = 10 rpm, variation change frequency = 59 Hz.

Table 2
Standard deviation, normalized by theoretical segment, of the encoder circumference ratio computed from Eq. (8) with non-constant shaft speed the operational specifications: encoder segments, $N = 180$; base running speed, $f_{\text{shaft}} = 30\,\text{Hz}$; zero crossing clock, $f_{\text{clock}} = 80\,\text{MHz}$; shaft revolutions averaged, $m = 50$

Shaft speed variation amplitude (revolutions/min)	Shaft speed variation change rate (Hz)	Normalized standard deviation
2	120	4.48×10^{-6}
5	120	4.72×10^{-6}
10	120	6.75×10^{-6}
10	10	4.24×10^{-6}
10	28.2	4.09×10^{-6}

running speed change) to that obtained for ideal conditions (i.e., one revolution at a constant speed). This result indicates that the encoder calibration is a robust process over the range of operating conditions examined. These conditions were chosen to reflect conditions encountered in typical rotating equipment applications.

6. Experimental evaluation

The encoder quantification, Eq. (11) and compensation scheme, Eq. (16), can be used to improve the quality of torsional vibration measurements acquired with less than ideal transducers. To evaluate the performance, the process has been implemented in four applications with different types of shaft encoding devices as shown in Fig. 8. The synchronous averaged encoder geometry (Eq. (10) with 50 revolutions) is shown for each installation. For reference, the theoretical encoder segment circumference ($1/N$) is also shown for each system. Each of the respective circumference ratio graphs is displayed with a range of $\pm 20\%$ of the theoretical value to enable a visual quantitative comparison between the encoders. Inspection of the data in Fig. 8 yields the following observations for each of the four respective installations:

1. The measurement device in Fig. 8(a) is 2048 pulses-per-revolution (ppr) of the optical encoder (BEI Industries Model HS25) installed on a laboratory test stand. This encoder system is as close to the ideal situation as is possible with currently available technology. Hence, application of the compensation to this encoder is not expected to improve the results, but can be used to help establish the performance limits of the compensation scheme with other encoders.
2. The encoding device in Fig. 8(b) is a laser printed zebra tape with 159 stripes installed on a 3 in (76.2 mm) diameter disk attached to a rotating shaft on another laboratory test stand. Significant variation is apparent in the encoder segments. In particular, note that the 60th index is considerably larger than the others and this is due to the end effect. The end effect is visually apparent in the photograph of the zebra tape installation in Fig. 8(b). Also, note that approximately every 9th stripe is slightly larger than the others. This is a result of the laser printer resolution. The average value of the fractional stripe width for approximately every 9th

stripe is 0.643%, or 0.0606 in on a 3 in diameter shaft. The other stripes average about 0.628%, or 0.0592 in on a 3 in diameter shaft. On a 600 dpi printer, these widths correspond to 37 and 36 lines of print per stripe, respectively. Hence, an extra line is printed every 9 stripes. This pattern is still apparent after the synchronous averaging (Eq. (11)), as seen in Fig. 8(b).

3. Fig. 8(c) shows pulse width measurements for a 60 toothed-gear speed encoder installed on a high-speed turbo-machine (10,000 revolutions/min). The quality of machining on the gear is fairly consistent; however, variations from the nominal are apparent.
4. Fig. 8(d) shows the averaged interval measurements from a specially machined 180 tooth encoder on a laboratory test stand. The banded variation above and below the theoretical is apparent.

The synchronous averaging method shows that each encoder system has an underlying geometric pattern. The optical encoder has a low level of variance as would be expected from the

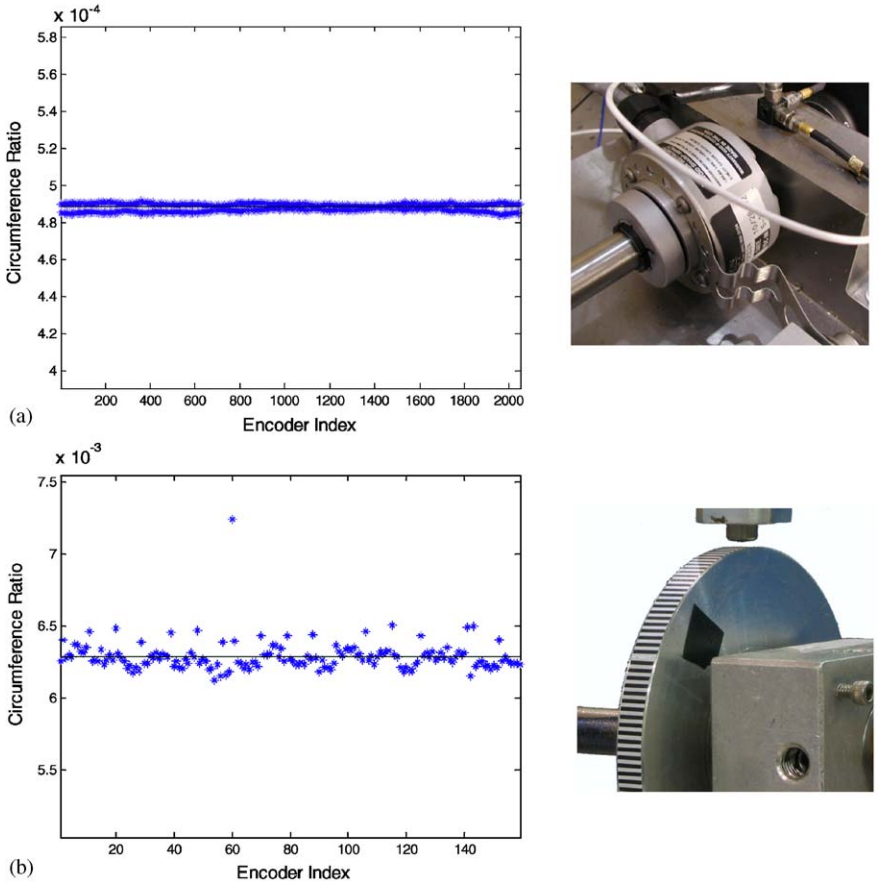

Fig. 8. Shaft encoding devices and in situ measured circumference ratio from Eq. (8); +, the measured circumference ratio; ——, evenly spaced theoretical circumference ratio: (a) 2048 increment optical encoder on a laboratory test stand; (b) 159 stripe laser printed zebra tape on a laboratory test stand; (c) 60 tooth timing wheel on gas turbine test rig; (d) 180 tooth specialized encoder wheel on a laboratory test stand.

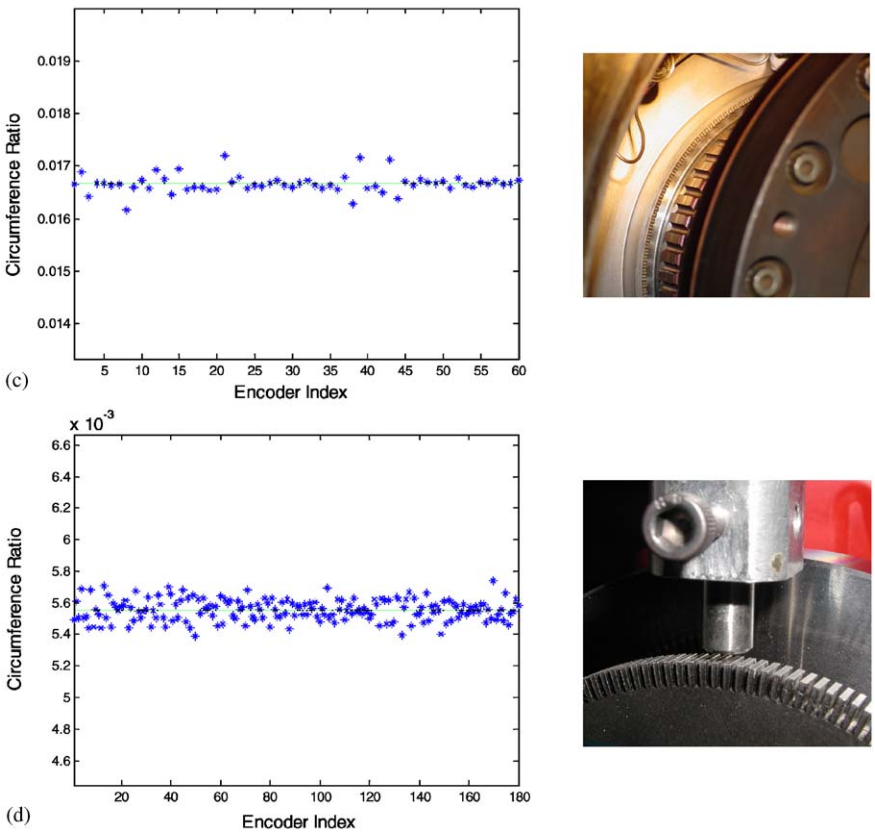

Fig. 8. (*Continued*)

high level of precision used in its manufacturing. The other encoder systems show different degrees of variation between angular intervals. The variation was most prominent with the printing and installation of the zebra tape. The effects that the variation has on the torsional vibration and the ability to correct for it are explored in the next section.

7. Torsional vibration measurement

7.1. Laboratory test bed with 2048 optical encoder

To establish a baseline, tests were performed on a laboratory test bed to illustrate the capabilities of the encoder correction method. The test bed consisted of a shaft system supported by two impregnated journal bearings driven by a 12 horsepower variable speed DC motor. The optical encoder shown in Fig. 8(a) was used to acquire the time intervals. The passage times were detected with a National Instruments PCI-6602 Timer/Counter Board using an 80 MHz clock reference. The motor was operated at approximately 3000 revolutions/min for approximately 90 s

and the passage data acquired. Eqs. (1)–(3) were used to compute the torsional vibration signal. The signals were converted to the time domain assuming constant rotational speed. A Hanning window was applied to each of 50 2^{17} point arrays. A discrete Fourier transform was taken for each respective window array with an FFT algorithm. The 50 transforms were averaged to estimate the spectrum.

The lower-frequency range the spectral torsional oscillations is shown in Fig. 9(a) [19]. The strong harmonic content apparent in the spectrum is actually a result of the motor speed control and not an artifact of the torsional processing. The system's first torsional natural frequency is slightly less than 150 Hz and is apparent as one of the double peaks in that region. Next, the in situ encoder circumferential ratio compensation (Fig. 8(a)) was used with Eq. (16). The two spectra

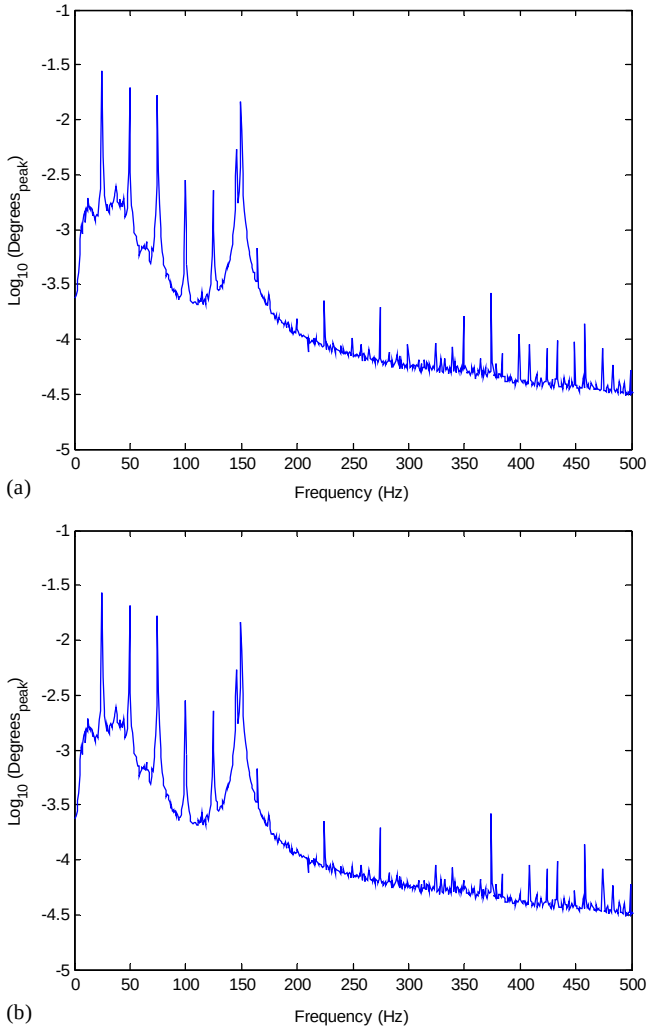

Fig. 9. Torsional vibration spectrum from laboratory test stand with 2048 ppr optical encoder: (a) direct processing of encoder signal, with constant speed assumption; (b) with encoder compensation and constant shaft speed assumption.

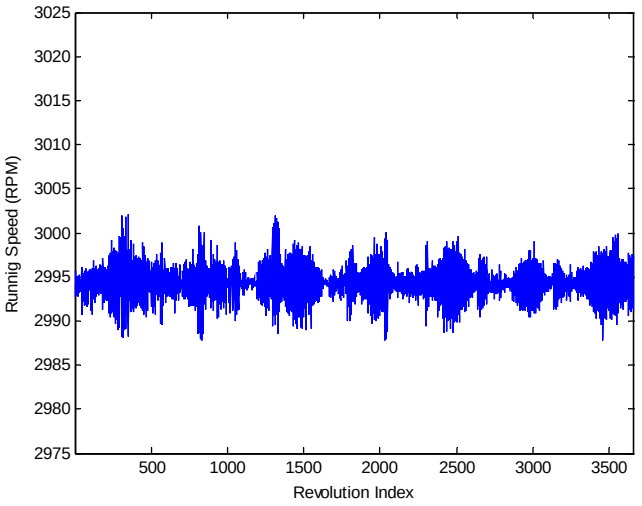

Fig. 10. The shaft running speed over data acquisition period from laboratory test with 2048 ppr optical encoder.

are virtually identical with only minor differences apparent. Therefore, with this high precision optical encoder the interval variation is not an issue.

The measured shaft speed for approximately 3800 revolutions is shown in Fig. 10. Close inspection shows that the shaft can experience speed changes in the range of 10 revolutions/min in within 50 revolutions. Recall that in the spectrum calculation one FFT data block contains 2^{17} points, which means 64 shaft revolutions are needed to fill the array. A change of this magnitude calls into question the assumption that the shaft speed is constant throughout a single revolution. The 2048 ppr optical encoder torsional vibration data was reprocessed with encoder compensation and constant time interval resampling. The spectrum is shown in Fig. 11. In general, the spectrum is similar to Fig. 9, computed without the resampling. However, closer inspection around the 150 Hz region shows differences, in that the "skirts" adjacent to the peaks have been reduced. This reduction indicates that the speed change is sufficient to induce this frequency smearing artifact.

Analysis of this torsional vibration data acquired with a high-quality optical encoder allows several observations to be made. (1) The encoder segment variation has little effect on the data. (2) Application of the encoder compensation is neither beneficial nor harmful to the spectral estimate. (3) The constant time resampling is beneficial in improving the spectral estimate. Frequency smearing due to running speed variations is reduced.

7.2. *High-speed turbo-machine with 60 tooth gear encoder*

Fig. 8(c) shows a 60 tooth gear encoder on a high-speed (10,000 rpm) turbo machine. The sensor used to detect the gear teeth passage is a Hall effect transducer. Note, that the Hall effect is not visible in the photograph. A timer/counter with a 19.6 MHz clock rate was used to capture the respective passage times of each tooth. Approximately, 90 s of data from about 15,000 revolutions was acquired.

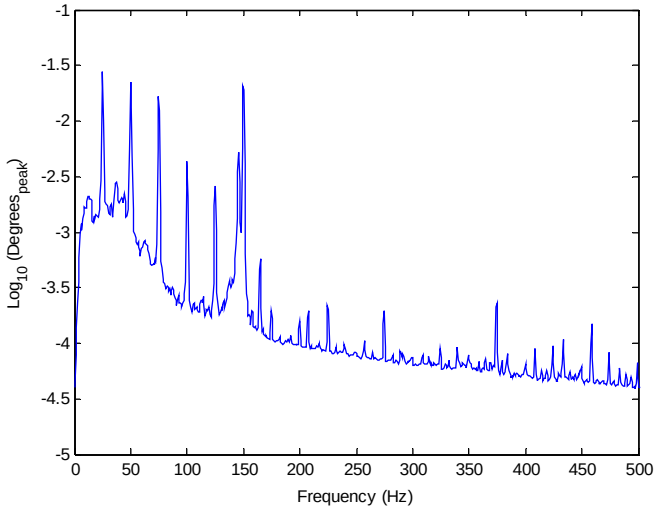

Fig. 11. Torsional vibration spectrum from laboratory test stand with 2048 ppr optical encoder with encoder compensation and constant time interval resampling.

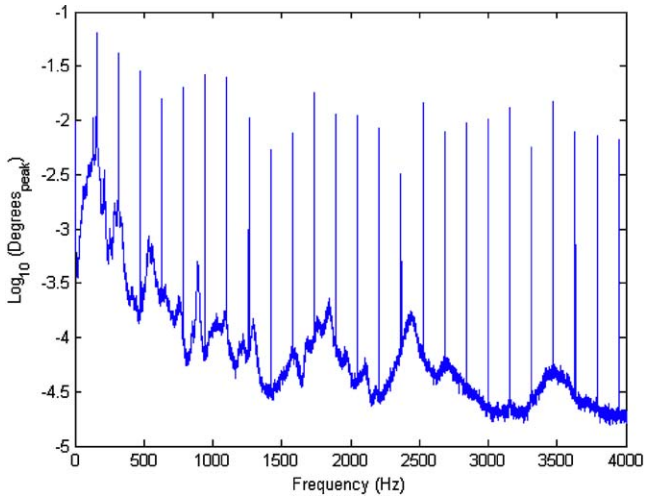

Fig. 12. Torsional vibration of high-speed turbo-machine measured with a gear encoder (Fig. 8(c)), the digital time interval measurement method.

The torsional vibration was initially estimated directly from the passage time array using Eq. (2). The frequency spectrum was estimated with a Hanning window and 50 ensemble averages, with an FFT block size of 2^{17}. The spectrum, shown in Fig. 12, has high amplitude content at multiples of the running speed (approximately 160 Hz). The order spectra computed from Eq. (19) is shown in Fig. 13. Inspection confirms that the high amplitude tonal content occurs at exact integer multiples of the running speed and is caused by the variations in the encoder teeth spacing.

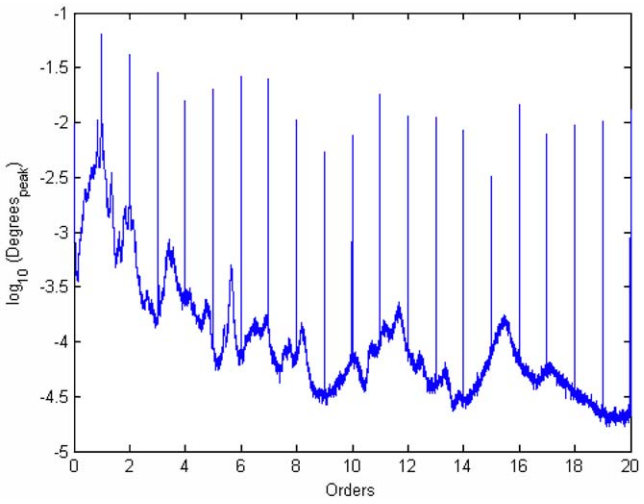

Fig. 13. Torsional vibration order spectrum of a high-speed turbo-machine via the digital time interval measurement method.

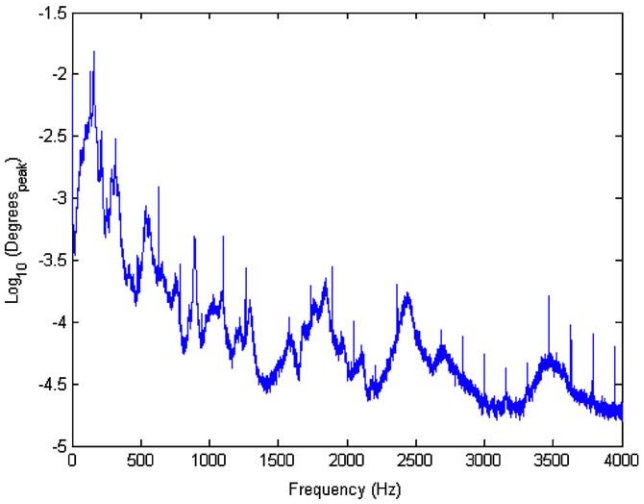

Fig. 14. Torsional vibration spectrum of high-speed turbo-machine in using encoder interval correction via the digital time interval measurement method.

Next, the data was reprocessed using the synchronous averaged circumference ratio and Eq. (18) to compute the torsional vibration. The spectrum was estimated using the procedure previously described and is shown in Fig. 14. It shows a marked reduction in the order content from the original torsional spectrum shown in Fig. 12. Unlike the optical encoder, the gear teeth variations are sufficient to induce significant corrupting effects. Furthermore, the proposed compensation scheme works reasonably well, significantly reducing the high order content

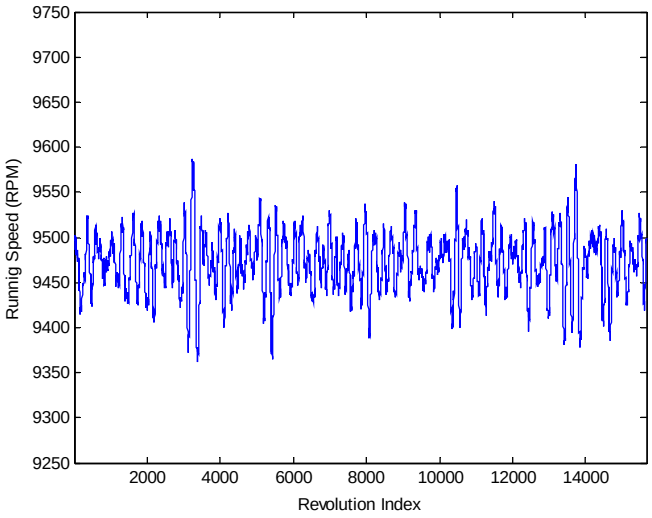

Fig. 15. Shaft running speed of high-speed turbine during acquisition of torsional vibration.

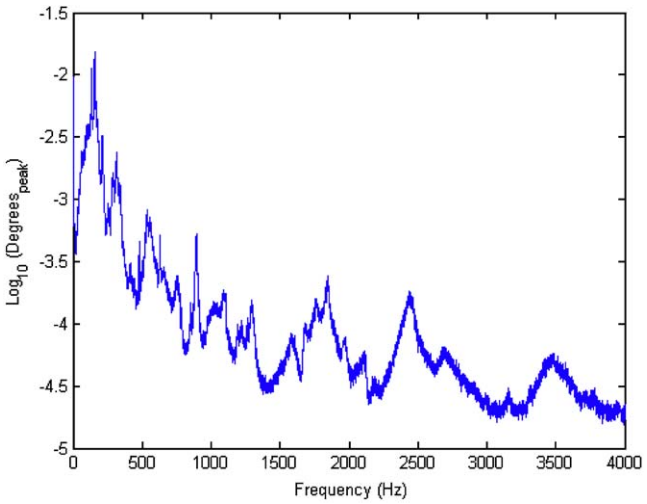

Fig. 16. Torsional vibration spectrum of high-speed turbo-machine using encoder interval correction, and constant time resampling via the digital time interval measurement method.

induced by the irregular spacing of the encoder teeth. However, close inspection show that some low level order components remain, particularly in the higher frequencies.

The shaft running speed is shown in Fig. 15 and reveals that significant speed changes occur. Speed changes of up to 200 revolutions/min over as few as 120 revolutions were observed. The constant time interval resampling routine was applied and the resulting spectrum computed. The result is shown in Fig. 16. There is a further elimination of the low-level corrupting order content

that was apparent in Fig. 14. The removal of the order artifacts by resampling confirms that the shaft speed is changing sufficiently to violate the constant speed assumption. The application of the order reduction process has now made the interpretation of the torsional vibration spectrum much easier than the original in Fig. 12. The following observations can be made for this test:

1. Geometric errors from devices such as gears can be sufficient to induce high-level order content in the torsional vibration spectrum. The artifacts are even greater in amplitude for more irregular encoding devices, such as zebra tape (Fig. 8(b)). The encoder compensation method can be very effective in reducing the artifacts.
2. Running speed variations can be sufficiently significant to induce non-uniform time based sampling, thus affecting the spectrum. The constant time resampling is effective in reducing the artifacts.

8. Summary

High amplitude order content introduced from measurement and/or processing of torsional vibration signals can obscure features in the torsional vibration spectra. The root cause of the corrupting orders is usually a combination of the shaft encoding device and operating conditions. Unless a precision optical encoder is used, the encoders lack incremental uniformity. Even small geometric variations can introduce unwanted order content. If the shaft running speed changes throughout a revolution, the torsional vibration signal is acquired with a non-constant interval time basis and can introduce errors.

An in situ characterization of the encoder was developed by using synchronous averaging. The characterization is used to correct the non-uniform circumferential geometry providing a more accurate reference to compute the angular deflection. A simulation study showed that fifty averages were sufficient to compute an accurate circumference ratio. The characterization method was applied to data from four different experimental tests to examine the errors and the ability of the proposed method to minimize them. The following conclusions are drawn from the study:

1. The geometric interval variation of precision optical encoders is insufficient to create sampling artifacts in the spectra.
2. Less precise encoders such as time gears can be significantly corrupted by order content directly caused by the encoder geometric variability. The corruption manifests itself as order content up to 50–60 dB greater than the underlying torsional vibration of interest.
3. Adhesive backed printed zebra tape encoding schemes possess a number of problems leading to high-level corrupting order content. Possible error genesis includes: (1) non-uniformity in stripe printing caused by printer resolution, (2) tape end installation effects, and (3) non-uniformity (i.e., waviness) in the orientation of the tape around a large diameter shaft.

The encoder correction method was beneficial in greatly reducing artifacts induced by the encoder. Application of the order correction method to the precise encoder data did not adversely affect the results. It may be concluded that when the method is applied the results will only be improved and is therefore generally recommended for equipment in which the torsional vibration

is not synchronized with the shaft position. Under conditions when the torsional vibration is synchronized with shaft position, such as in an internal combustion engine the method as developed here is not directly applicable. Furthermore, the time encoder averaging process may adversely affect any torsional vibration that is synchronized with shaft position. Hence, as developed, caution is urged in situations when there is the likelihood of synchronous excitation and vibration.

Since the geometric correction method is performed in situ it may be applied regularly to adjust for changes in the encoder through normal operation. For example, as a shaft's temperature changes thermal expansion can change some encoder (i.e., gears and tape) segment dimensions. The in situ method can be easily implemented in these situations.

Variations in encoder geometry and changes in shaft running speed cause the torsional vibration to be computed at time intervals that are not constant. The non-regular sampling induces difficulties when using constant interval-based discrete Fourier transform algorithms with these arrays. A resampling interpolation algorithm based on the work in Ref. [20] was applied to create a constant interval array. The results showed:

1. There was a reduction in frequency smearing effects from running speed variations even with precision optical encoders.
2. Corrupting order artifacts on a high-speed turbo machine with a timing gear encoder with application of the encoder were eliminated when the encoder correction and resampling was applied.

Combination of synchronous averaging encoder compensation and constant time interval resampling are effective in significantly improving the quality of time interval torsional vibration measurement. The improved torsional vibration spectra can now be used in demanding applications that require the harvesting of fine spectral features, such as continuous machinery health monitoring.

Acknowledgements

This work was supported by the Penn State Applied Research Laboratory Exploratory and Foundational Program; the *Multi-disciplinary University Research Initiative for Integrated Predictive Diagnostics* (Grant No. N00014-95-1-0461) sponsored by the Office of Naval Research and; NASA Glenn/GE Aircraft Engines *Turbine Disk Crack Detection Using Torsional Vibration: A Feasibility Study* (GEAE Purchase Order 200-1X-14H45006). The content of the information does not necessarily reflect the position of the USA Government, and no official endorsement should be inferred.

References

[1] S.J. Citron, J.E. O'Higgins, L.Y. Chen, Cylinder by cylinder engine pressure and pressure torque waveform determination utilizing speed fluctuations, SAE Paper No. 890486, 1989.

[2] D. Remond, Practical performance of high-speed measurement of gear transmission error or torsional vibrations with optical encoders, *Measurement Science and Technology* 3 (9) (1998) 347–353.
[3] R.L. Rouston, J.M. Starkey, P. Wang, P. Davies, Torsional and translational vibrations of a drive shaft with a cardan joint, *American Society of Mechanical Engineers, Flexible Mechanisms, Dynamics, and Analysis* DE-47 (1992) 533–542.
[4] K.P. Maynard, M.W. Trethewey, On the feasibility of blade crack detection through torsional vibration measurements, *Noise and Vibration Worldwide* 31 (2000) 9–15.
[5] H. Diangui, Experiment on the characteristics of torsional vibration of rotor-to-stator rub in turbomachinery, *Tribology International* 33 (2000) 75–79.
[6] G. Szász, E.J. Guindon, Using torsional vibration spectra to monitor machinery rotor integrity, *Proceedings of the ASME 2003 International Joint Power Conference, ASME* Paper No. IJPGC2003-40162, Atlanta, GA, USA, 2003.
[7] N.A. Halliwell, C.J.D. Pickering, P.G. Eastwood, The laser torsional vibrometer: a new instrument, *Journal of Sound and Vibration* 93 (1984) 588–592.
[8] X. Li, L. Qu, G. Wen, C. Li, Application of wavelet packet analysis for fault detection in electro-mechanical systems based on torsional vibration measurement, *Mechanical Systems and Signal Processing* 17 (6) (2003) 1219–1235.
[9] Honeywell Sensotec, 2080 Arlington Lane, Columbus, OH, USA, 2003.
[10] S. Seidlitz, Engine torsional transducer comparison, SAE Paper No. 920066, 1992.
[11] H. Fu, P. Yan, Digital measurement method on rotating shaft torsional vibration, *American Society of Mechanical Engineers, Vibration of Rotating Systems* DE-60 (1993) 271–275.
[12] P. Wang, P. Davies, J.M. Starkey, R.L. Rouston, A torsional vibration measurement system, *IEEE Transactions on Instrumentation and Measurement* 41 (6) (1992) 803–807.
[13] W. Hernandez, D. Paul, Vosburgh, on-line measurement and tracking of turbine torsional vibration resonances using a new encoder based rotational vibration method (RVM), Society of Automotive Engineers Paper No. 961306, 1996.
[14] CoppTek, Barrington, IL, USA, 2003.
[15] J.M. Vance, *Rotordynamics of Turbomachinery*, Wiley, New York, 1988 pp. 379–383.
[16] J. Williams, Improved methods for digital measurement of torsional vibration, SAE Paper No. 962204, 1996.
[17] K.P. Maynard, M.W. Trethewey, R.S. Gill, B.R. Resor, Gas turbine blade and disk crack detection using torsional vibration monitoring: a feasibility study, *Proceedings of 14th International Congress and Exhibition on Condition Monitoring And Diagnostic Engineering Management (COMADEM)*, University of Manchester, UK, 2000.
[18] P. Wang, P. Davies, J.M. Starkey, R.L. Routson, Torsional mode shape measurements on a rotating shaft, *Proceedings of the 10th International Modal Analysis Conference*, 1992, pp. 676–682.
[19] B.R. Resor, Processing and modeling of torsional vibration for turbine blade crack diagnostics, M.S. Thesis, Department of Mechanical and Nuclear Engineering, The Pennsylvania State University, 2002.
[20] C.L. Groover, M.W. Trethewey, K.P. Maynard, M.S. Leebold, Removal of order domain content in rotating equipment signals by double resampling, *Mechanical Systems and Signal Processing* 19 (3) (2005) 483–500.